ACS OMEGA

Article

http://pubs.acs.org/journal/acsodf

Enhanced Peripheral Nerve Regeneration by a High Surface Area to Volume Ratio of Nerve Conduits Fabricated from Hydroxyethyl Cellulose/Soy Protein Composite Sponges

Yanteng Zhao,[†,‡] Qiang Zhang,[†] Lei Zhao,[†] Li Gan,[†,§] Li Yi,[†] Yanan Zhao,[†] Jingling Xue,[†] Lihua Luo,[∥] Qiaoyue Du,[†] Rongxin Geng,[†] Zhihong Sun,[†] Nadia Benkirane-Jessel,[⊥,#] Pu Chen,[†] Yinping Li,*[,†] and Yun Chen*[,†]

[†]Department of Biomedical Engineering, School of Basic Medical Sciences, Wuhan University, Wuhan 430071, China

[‡]Department of Transfusion, The First Affiliated Hospital of Zhengzhou University, Zhengzhou 450052, China

[§]Department of Cell Biology, School of Medicine, Wuhan University of Science and Technology, Wuhan 430065, China

[∥]Laboratory of Stem Cells and Tissue Engineering, School & Hospital of Stomatology, Wenzhou Medical University, Wenzhou 325027, China

[⊥]INSERM (French National Institute of Health and Medical Research), Osteoarticular and Dental Regenerative Nanomedicine Laboratory, UMR 1109, Faculté de Médecine, Strasbourg F-67000, France

[#]Université de Strasbourg, Faculté de Chirurgie Dentaire, 1 place de l'Hôpital, Strasbourg F-67000, France

ABSTRACT: Multichannel nerve guide conduits (MCNGCs) have been widely studied and exhibited outstanding nerve repair function. However, the effect of the geometric structure of MCNGCs on the nerve repair function was still not clear. Herein, we postulated that MCNGCs with different inner surface area-to-volume ratios (ISA/V) of the channels inside the nerve guide conduits (NGCs) would show different nerve repair functions. Therefore, in current work, we constructed a series of hydroxyethyl cellulose/soy protein sponge-based nerve conduit (HSSN) with low, medium, and high ISA/V from hydroxyethyl cellulose (HEC)/soy protein isolate (SPI) composite sponges, which were abbreviated as HSSN-L, HSSN-M and HSSN-H, respectively. These NGCs were applied to bridge and repair a 10 mm long sciatic nerve defect in a rat model. Finally, the influence of ISA/V on nerve repair function was evaluated by electrophysiological assessment, histological investigation, and in vivo biodegradability testing. The results of electrophysiological assessment and histological investigation showed that the regenerative nerve tissues bridged with HSSN-H and HSSN-M had higher compound muscle action potential amplitude ratio, higher percentage of positive NF200 and S100 staining, larger axon diameter, lower *G*-ratio, and greater myelination thickness. Furthermore, the regenerative nerve tissues bridged with HSSN-H also showed higher density of regenerated myelinated nerve fibers and more number of myelin sheath layers. On the whole, the repair efficiency of the peripheral nerve in HSSN-H and HSSN-M groups might be better than that in HSSN-L. These results indicated that higher ISA/V based on HEC/SPI composite sponge may result in greater nerve repair functions. The conclusion provided a probable guiding principle for the structural designs of NGCs in the future.

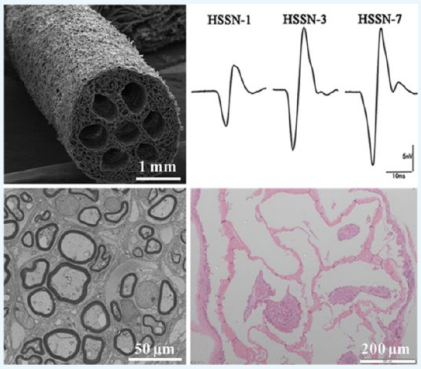

INTRODUCTION

Peripheral nerve lesions often cause the lack of sensory and motor functions, decreasing the life quality of patients.[1] In clinic, numerous surgeries have been carried out each year for repairing nerve injury. For short defects, end-to-end coaptation is an appropriate treatment in nerve injury.[2−4] However, when the nerve lesion is extensive (≥10 mm), a graft is needed to bridge the transected nerve.[5,6] The graft not only provides the structural support to stabilize the injury and architecture to direct axonal elongation but also supports cell infiltration and limits the scar formation.[1,7] Unfortunately, it is still hard to achieve the complete recovery of nerve functions. Although the autologous nerve graft is the gold standard in nerve repair, it also has several limitations, such as the need of an extra incision, the loss of the donor nerve function, limited availability of the donor nerve, and mismatch in size between the donor nerve and the injured nerve.[8−10] Therefore, the substitution of autograft is demanded to repair extensive nerve lesion.

With the development of tissue engineering, the nerve guide conduits (NGCs) have provided a promising alternative for nerve repair without sacrificing natural nerves.[11] NGCs provide a permissive chamber for nerve regeneration, preventing the invasion of fibrous tissue and allowing the transected stumps

Received: July 16, 2017
Accepted: October 19, 2017
Published: November 1, 2017

DOI: 10.1021/acsomega.7b01003
ACS Omega 2017, 2, 7471−7481

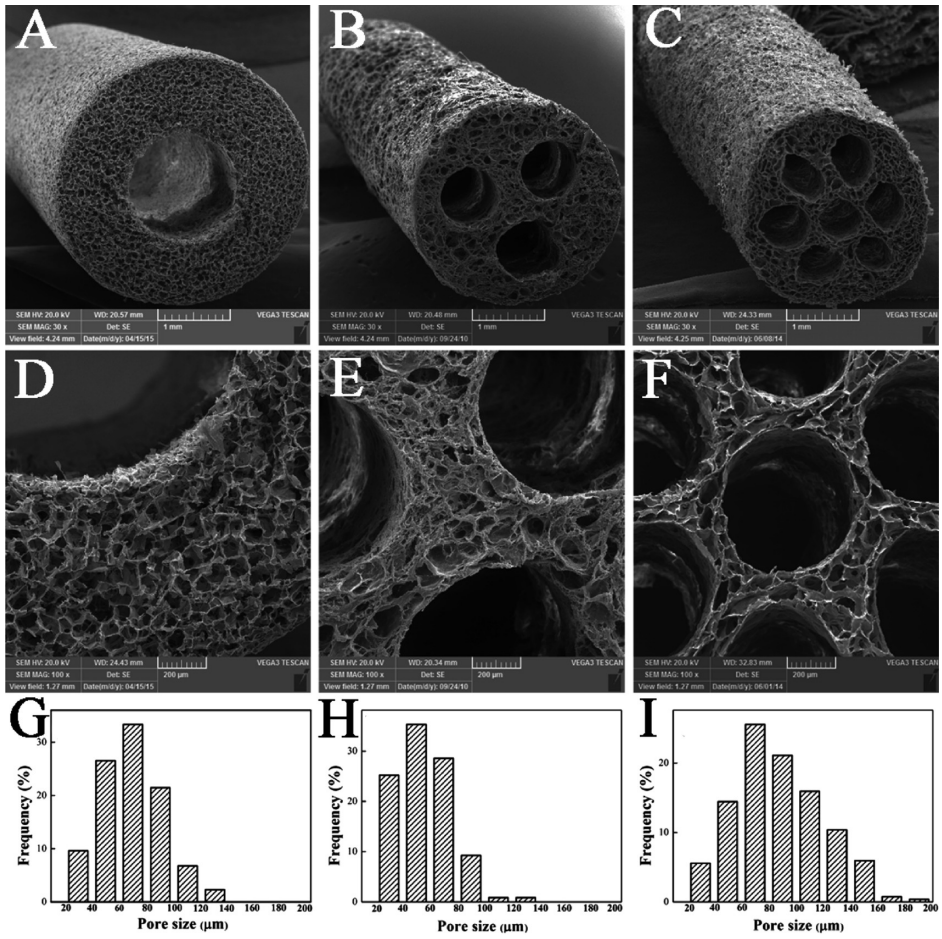

Figure 1. SEM images of the HSSN-L (A, D), HSSN-M (B, E), and HSSN-H (C, F). Porosity distribution of the HSSN-L (G), HSSN-M (H), and HSSN-H (I); n = 10.

sprouting in the lumen.[1] In the past decades, natural or synthetic biomaterials had been applied to construct NGCs and exhibited considerable nerve repair function in experimental and clinical work. At first, the structure design of NGCs was mainly focused on single lumen. However, recent studies have indicated that multichannel NGCs (MCNGCs) were superior to NGCs with a single channel in nerve repair. This can be explained as follows:[10,12−19] (1) the longitudinally arranged channels inside the conduits can function as required microtubes with large surface areas for the synthesis of lamina basalis and impose significantly positive effects on neurite extension and attachment, proliferation, and migration of Schwann cells; (2) inside the conduits, the multiple channels orientated lengthways are capable of reducing the dispersion of axonal branches and in turn promote axonal elongation; and (3) the longitudinally arrayed multiple channels can reduce the misdirection ratio of regrown axons or polyinnervation of various targets. Therefore, MCNGCs have been regarded as more suitable candidates than NGCs with a single channel.

From the existing studies,[10,20] the regeneration process of peripheral nerve was influenced not only by the number and diameter of channels inside the MCNGCs but also by the inner surface area of the channels inside the MCNGCs. However, among the above factors, the factor which played a key role in influencing the scaffold performance and nerve regeneration was still not clear. Several studies have shown that the inner surface area-to-volume ratio (ISA/V) of the channels inside the NGCs could systematically reflect the influence of diameter, cross-sectional area, and surface area of the channels inside the MCNGCs on nerve repair.[20−23] These studies prompted us to investigate the ISA/V of the channels inside the NGCs. In addition, it has been indicated that melt-spun fibers with a high ISA/V promote efficient cell seeding and subsequent cell proliferation, which facilitate the nutrient transportation and spatial distribution of cells.[21] In addition, a high ISA/V provides a suitable microenvironment for biological elements (e.g., enzymes, antibodies, nucleic acids, cells, and tissue sections).[24] Thereupon, we postulated that the MCNGCs with a larger ISA/V would show better nerve repair efficiency, whereas the smaller diameter and larger inner surface area of the channel inside the MCNGCs could promote nerve regeneration. Moreover, if the tunable degradation rate of NGCs can match the rate of nerve regeneration, it will avoid a second surgical procedure and show great advantages in the process of nerve repairing.[9]

In our previous study, we fabricated a series of hydroxyethyl cellulose (HEC)/soy protein isolate (SPI) composite films.[25] The composite films exhibited a relatively high mechanical strength, an adjustable water uptake ratio and moisture absorption ratio, biocompatibility, and controlled degradation rate in vitro and in vivo, indicating a great potential for biomedical applications. Additionally, our other work has demonstrated that cellulose/SPI composite sponge NGCs have better nerve repair function than cellulose/SPI composite film

DOI: 10.1021/acsomega.7b01003
ACS Omega 2017, 2, 7471−7481

Table 1. Code and Geometrical Parameters of Different MCNGCs

samples	number	outer diameter (mm)	channel diameter (mm)	cross-sectional area (mm^2)	inner surface area (mm^2)	volume (mm^3)	inner surface area to volume ratio (ISA/V) (mm^{-1})
HSSN-L	1	3.5	1.5	1.77	56.52	21.20	2.67
HSSN-M	3	3.5	0.8	1.51	90.43	18.09	5.00
HSSN-H	7	3.5	0.5	1.37	131.88	16.49	8.00

NGCs.[26] Because of the higher biodegradability of HEC than cellulose, we supposed that the NGCs fabricated from the HEC/SPI composite sponge would be promising in nerve repair. Because of the difficulty in varying only one parameter without varying other structural parameters, it is hard to design and control the geometrical factors of NGCs. Therefore, to verify our hypothesis, we prepared a series of HEC/SPI-based MCNGCs with different ISA/V by adjusting the number and diameter of the channels using our handmade mold. Finally, the nerve repair function of these MCNGCs was evaluated in an extensive nerve lesion rat model with regards to the commonly adopted parameters of peripheral nerve regeneration by using a variety of histological and electrophysiological techniques.

RESULTS

Structure of HSSN (Hydroxyethyl cellulose/soy protein sponge-based nerve conduit). Scanning electron microscopy (SEM) images and porosity distribution of HSSN-L, HSSN-M, and HSSN-H are shown in Figure 1. These sponge conduits display a regular cylindrical shape with a homogeneous porous structure. The pore sizes of three types of conduits range from 20 to 200 μm. As shown in Figure 1, the pore size distribution of HSSN-H seemed to be shifted toward the higher pore size. This is mainly because the sponge was divided into more regions because of more channels during the fabrication of the sponge conduit. As a result, the water within the sponge was squeezed toward less space. Therefore, under freezing, ice crystals get bigger, resulting in a larger pore size. This kind of porous structure might be helpful for the nutrition and air exchange and cell or tissue invasion and might promote the biodegradability when these conduits are used as in vivo implantations. As shown in Table 1, according to the structure design in advance, all of the conduits have a length of 12 mm and an outer diameter of 3.5 mm, whereas the diameters of the inner channels in HSSN-L, HSSN-M, and HSSN-H were 1.5, 0.8, and 0.5 mm, respectively. As a result, the calculated ISA/Vs were 2.67 for HSSN-L, 5.00 for HSSN-M, and 8.00 for HSSN-H. Thus, the ISA/V increased with increasing numbers and decreasing diameters of the inner channels in the conduits.

Electrophysiological Evaluation. Representative compound muscle action potential (CMAP) recordings at the injured side in each group are shown in Figure 2A. Compound action potentials were clearly observed in HSSN-L, HSSN-M, and HSSN-H groups at 3 months after the surgery, indicating a functional recovery of the injured nerves. Both the CMAP amplitude (Figure 2A) and the calculated CMAP amplitude ratio (Figure 2B) in these groups increased with the increase of ISA/V. The CMAP amplitude ratios of HSSN-L, HSSN-M, HSSN-H, and autograft groups were 44.32 ± 4.93%, 53.62 ± 9.10%, 56.05 ± 5.79%, and 61.65 ± 5.34%, respectively. The CMAP amplitude ratio in the HSSN-L group was lower than that in the autograft group ($P < 0.05$). However, there was no significant difference in the average CMAP amplitude ratio among HSSN-M, HSSN-H, and autograft groups ($P > 0.05$). These results indicated that the recovery of electrophysiological

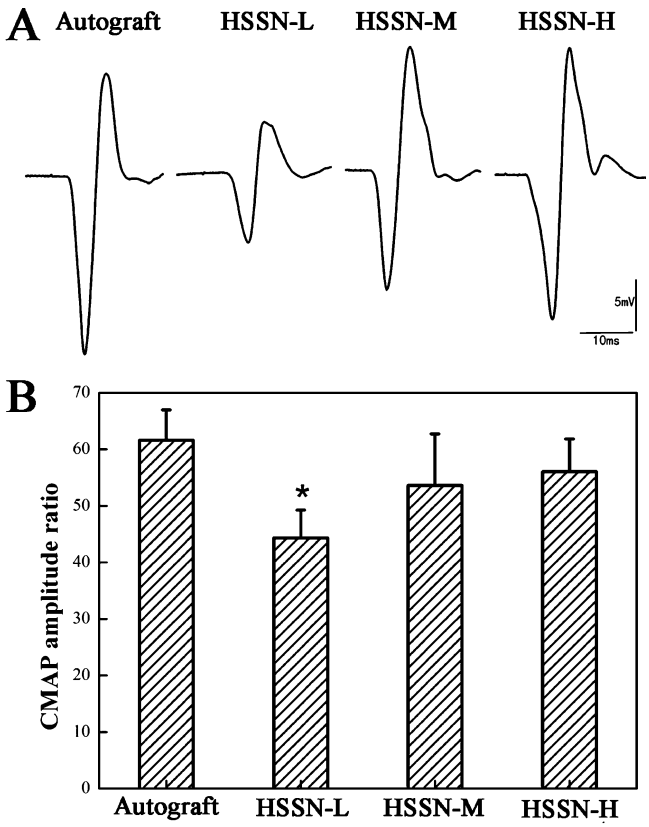

Figure 2. Representative CMAP recordings on the injured side for each group (A). The CMAPs were compared with the animal's contralateral control and expressed as the CMAP amplitude ratio (B). ($n = 10$; * $P < 0.05$, compared with autograft group).

properties in nerves bridged with HSSN-M and HSSN-H approached the autograft group and surpassed the HSSN-L group.

Histological Assessment of Regenerated Nerves. *HE Staining Analysis.* Three months after the surgery, the regenerative nerve tissues were harvested and stained by Hematoxylin-Eosin (HE). As shown in Figure 3, a bundle of newly regenerated nerve fibers extended inside the conduits from the proximal stump and aggregated to a fasciculate structure. A few new blood vessels (indicated by the black arrows) and connective tissues were observed in the regenerated nerve fibers. However, the distribution of the regenerated axons in the HSSN-L group was more scattered than that in HSSN-M and HSSN-H groups, indicating better regeneration of nerve fibers in HSSN-M and HSSN-H groups.

Double NF200 and S100 Immunofluorescence Analysis. Figure 4A shows the double NF200/S100 immunofluorescence image of the longitudinal section of the regenerated nerves. The immunopositivity percentages for NF200 and S100 presented the densities of axons and Schwann cells in the whole regenerative nerve bridged with HSSN-L, HSSN-M, and HSSN-H (Figure 4B). As shown in Figure 4A, the migrated

DOI: 10.1021/acsomega.7b01003
ACS Omega 2017, 2, 7471−7481

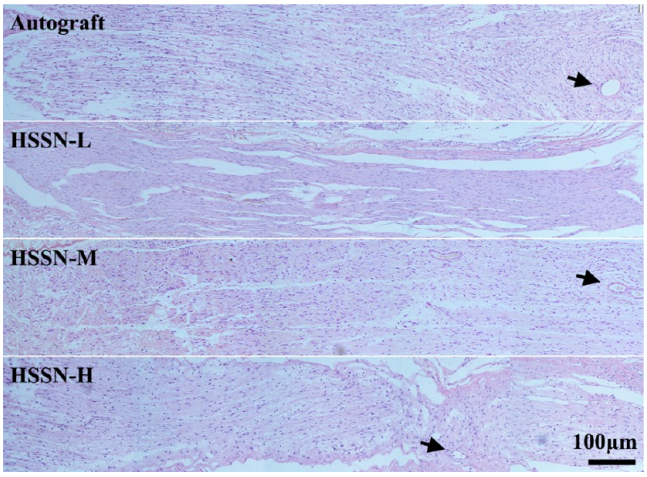

Figure 3. HE-stained images of longitudinal sections of regenerated nerves in each group. Black arrows present the newborn blood vessels, $n = 10$.

Schwann cells and regenerated axons were observed in all groups at 3 months after the surgery. Statistics of NF200-positive percentage indicated a significant difference between HSSN-L and autograft groups ($P < 0.05$), whereas the percentages of positive NF200 staining in both HSSN-M and HSSN-H groups were not significantly different from the autograft group ($P > 0.05$). Meanwhile, the average percentages of positive NF200 staining in HSSN-M and HSSN-H groups were higher than those in the HSSN-L group, whereas there was no significant difference between HSSN-M and HSSN-H groups.

Similar results were observed for S100 staining. The percentages of positive S100 staining in HSSN-L and HSSN-M groups were significantly lower than those in the autograft group ($P < 0.05$). But the percentage of positive S100 staining in the HSSN-H group was slightly lower than that in the autograft group ($P > 0.05$).

Toluidine Blue Staining and Electron Microscopy. Toluidine blue staining assay was performed to visualize myelin sheaths of the regenerated nerves. As shown in Figure 5A, cross section of the middle portion of the transplanted section in each group showed regenerated myelinated nerve fibers with different sizes and densities in each group. Three months after the surgery, the densities of myelinated nerve fibers in autograft, HSSN-L, HSSN-M, and HSSN-H groups were 15 250.53, 13 160.18, 11 865.31, and 13 384.94 per mm^2, respectively (Figure 5B). Although the HSSN-M group showed lower average density of myelinated nerve fibers than that in HSSN-L and HSSN-M groups, the difference in the total densities of myelinated nerve fibers among the HSSN groups was not statistically significant ($P > 0.05$), indicating that all HSSNs could mediate nerve regrowth.

Transmission electron microscopy (TEM) images of the cross section of the middle portion of the regenerated nerves are shown in Figure 6A. Three months after the surgery, the histomorphometric parameters of the regenerated nerves including axon diameter, myelin sheath thickness, *G*-ratio,

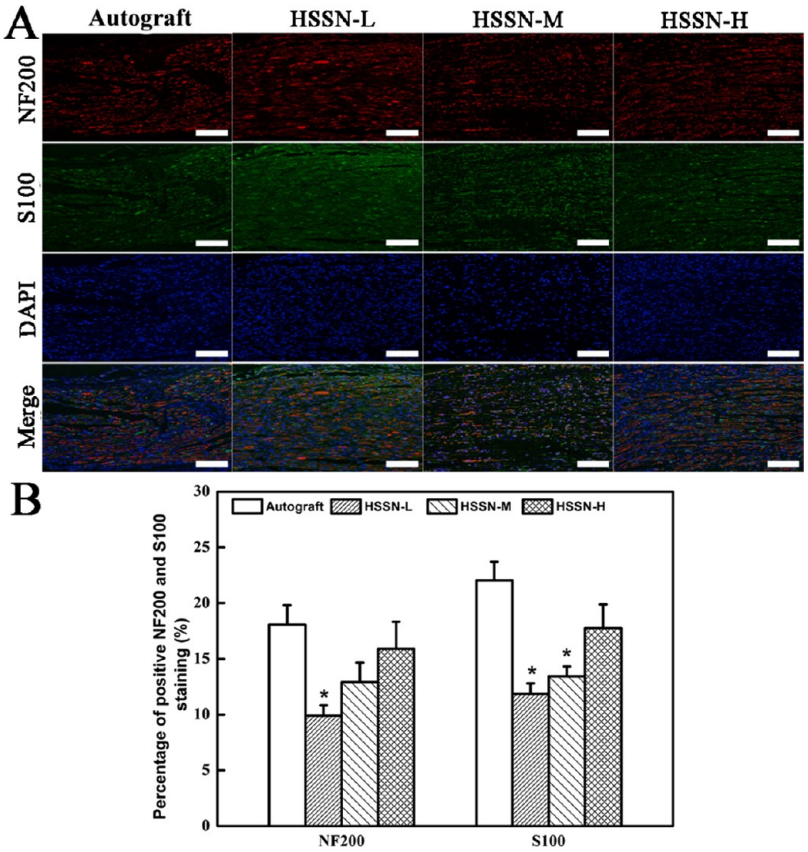

Figure 4. Double NF200/S100 immunofluorescence images of the longitudinal section of the regenerated nerves in each group at 3 months after the surgery (A). Statistical analysis of percentage of positive NF200 staining and positive S100 staining in each group (B). ($n = 10$; * $P < 0.05$, compared with autograft group). Scale bar, 100 μm.

DOI: 10.1021/acsomega.7b01003
ACS Omega 2017, 2, 7471−7481

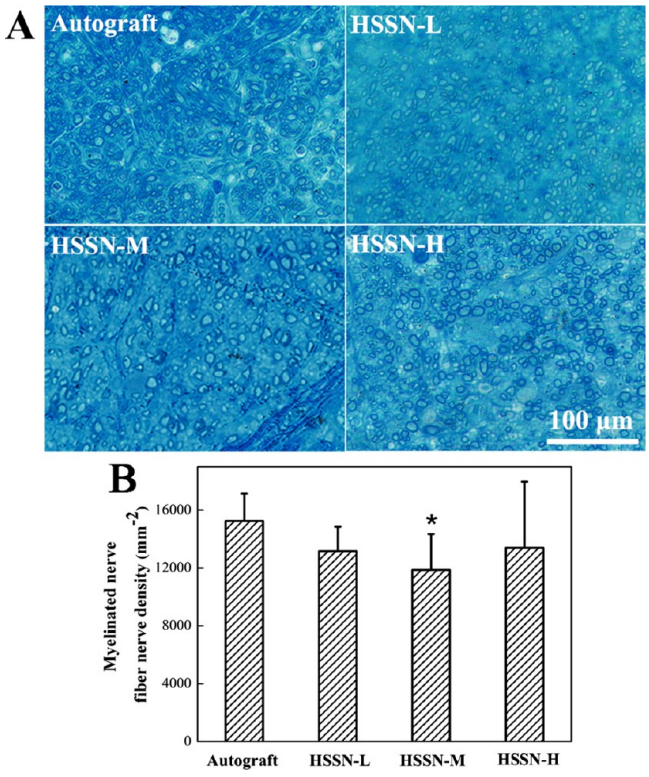

Figure 5. Toluidine blue staining of regenerated nerve cross-sections in the middle portion (A) and statistical analysis of myelinated nerve fiber density (B). (n = 10; * P < 0.05, compared with autograft group).

and the number of myelin sheath layers were investigated (Figure 6B). It was observed that the regenerated axons were surrounded by clear, thick, electron-dense myelin sheaths and a perfect basal membrane of Schwann cells in all groups. The myelin sheaths were characterized by abundant concentric circle structure layer by layer. A few myelinated fibers gathered into minifascicles, which were surrounded by a new perineurium. Similar to the autograft group, the structures of myelinated fibers of the regenerated tissues in the HSSN groups were compact. However, the regularly rounded myelinated fibers were seldom observed in HSSN-L and HSSN-M groups compared to those in HSSN-H and autograft groups. These results indicated that the group bridged with HSSN-H showed better morphology and function recovery of myelinated fibers, which was also demonstrated by the statistical data of the histomorphometric parameters of the regenerative nerves. The results revealed that the regenerative nerve tissues bridged with HSSN-H and HSSN-M showed larger axon diameter, lower G-ratio, and greater myelination thickness. In general, the ratio value measured in healthy nerves was around 0.7.[27] As a result, the G-ratio value of the HSSN-H group (0.77) in our work was very close to the normal G-ratio value of healthy nerves, indicating better axon regeneration than that in HSSN-L and HSSN-M groups. Furthermore, the regenerative nerve tissues bridged with HSSN-H also showed more number of myelin sheath layers. On the whole, the repair efficiency of the peripheral nerve in HSSN-H and HSSN-M groups might be better than that in HSSN-L, namely, the conduits with a higher ISA/V may have a better repair efficiency of the peripheral nerve.

Histological Assessment of Gastrocnemius Muscles. Three months after the surgery, the morphology of the rat gastrocnemius muscle was demonstrated by Masson trichrome staining and TEM analysis (Figure 7A). Muscles that have lost innervation usually suffer from atrophy, and the atrophy can be relieved accompanied with a gradual functional recovery of the sciatic nerves. As shown in Figure 7A, the muscle fibers were stained in red, whereas the collagen fibers were stained in blue. Similar to the autograft group, the HSSN-H group had wider muscle fibers which were parallel with each other (Figure 7A). As shown in Figure 7B,C, when the ISA/V increased, the cross-sectional areas of the muscle fibers increased, whereas the mean percentage of collagen fiber areas decreased. As a result, the sponge conduit with a larger ISA/V was easier to mitigate muscle atrophy than that with a smaller ISA/V in this case.

Degradation Analysis. The in vivo biodegradability of these sponge conduits was characterized by HE staining before and after implantation. As shown in Figure 8, three types of sponge conduits were dyed in red and the outer wall of HSSNs and the cavity of channels were apparently visible before implantation. For the original conduits (at 0 day), the integrated inner and outer walls of HSSNs could be clearly observed. The walls contain large amount of pores, which formed a spongelike structure of HSSNs. At 90 days after implantation, HSSNs severely deformed and the pores disappeared. The channel cavity of HSSNs was filled by the regenerative nerve tissue. Although the sponge matrix could still be observed, it was significantly decreased. In addition, at 90 days after implantation, the channel boundaries and the morphology of HSSN-L and HSSN-M were not distinguished clearly, whereas the thickness of the inner walls among channels and outer walls of HSSN-H decreased dramatically. These results revealed severe degradation of HSSNs.

DISCUSSION

In our previous work, a biodegradable and biocompatible HEC/SPI composite film has been reported.[25] Whether HEC/SPI composite materials could be used in nerve tissue engineering was investigated in this work. The reasons that we constructed MCNGCs from sponge were that the sponge structure could not only protect passages from radial compression, which prevents from collapse or blocking, but also provide better nutritional support and improve regeneration because of its high permeability.[28−30] Moreover, porous networks allow the transfer of growth factors and other soluble signaling molecules among cells in regenerating nerves.[14] Several studies have tried to model the architecture of NGCs, offering important guidelines about the diameter and inner surface area of the channel inside NGCs.[10,20,23,31] However, other geometrical key parameters are still missing, such as the ISA/V of the channel inside NGCs. The ISA/V is a comprehensive factor combining the diameter and cross-sectional area of the channels with the inner surface area of the channels inside the MCNGCs. Herein, we developed MCNGCs with different ISA/V based on HEC/SPI composite sponges using our handmade molds and then further investigated the effect of the ISA/V of the channel inside the MCNGCs on peripheral nerve regeneration.

CMAP test can offer an important index for studying the conducting function of the peripheral nerve. Regenerated nerve fibers must bridge the nerve gap and innervate the distal target muscle to produce a CMAP.[32] Because the amplitude of the CMAP positively correlated with the number of nerve fibers innervating the muscles, the diameter of axons, and the thickness of myelin sheath.[31,33] Therefore, the CMAP

DOI: 10.1021/acsomega.7b01003
ACS Omega 2017, 2, 7471−7481

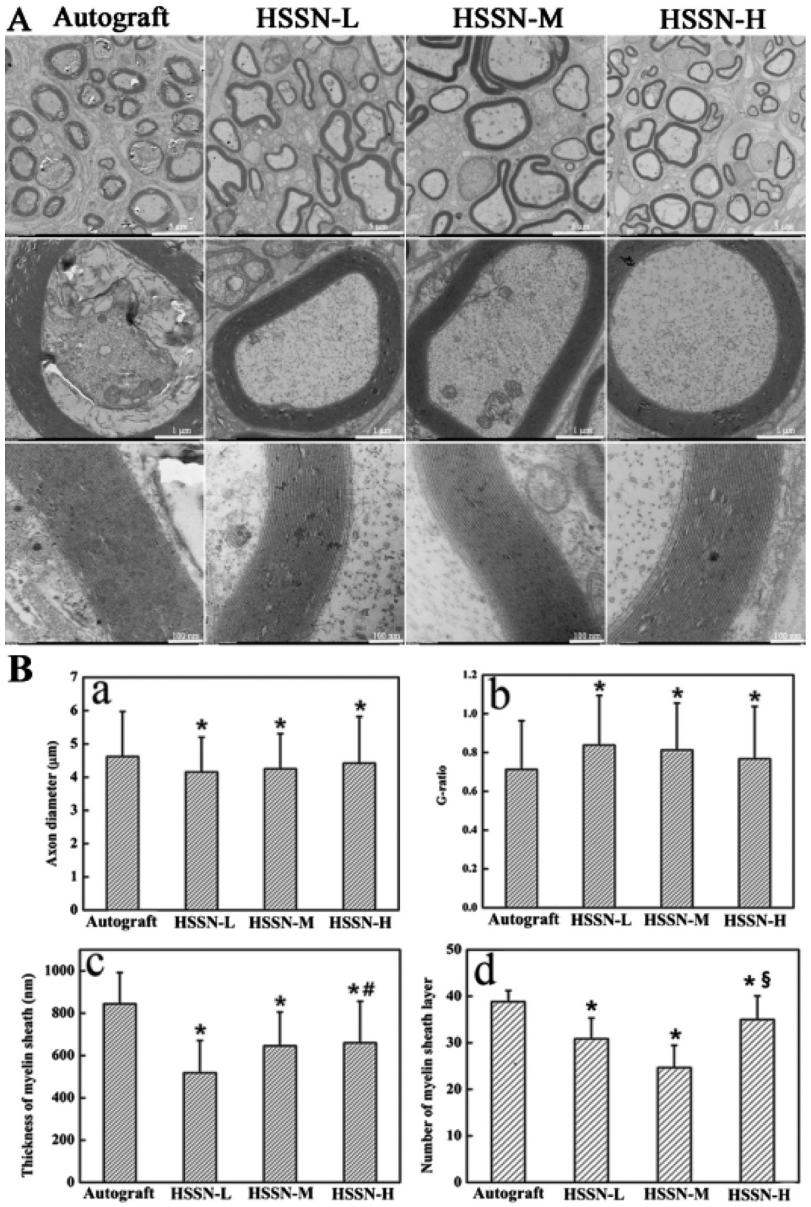

Figure 6. TEM images of the middle portion of regenerated nerve (A) and statistical analysis (B) of axon diameter (a), *G*-ratio (b), thickness of myelin sheath (c) and number of myelin sheath layer (d) calculated from TEM images for each group. * $P < 0.05$ (compared with autograft group); # $P < 0.05$ (compared with HSSN-L group); § $P < 0.05$ (compared with HSSN-M group). $n = 10$.

amplitude and the average CMAP amplitude ratio in a regenerated nerve are expected to be lower than that of a normal nerve. In this case, we observed CMAP in all groups, while the CMAP amplitude in the autograft group was the highest, indicating that the regenerated nerve function in conduit groups was partly recovered. In addition, the average CMAP amplitude ratio in HSSN-M and HSSN-H groups with a larger ISA/V was higher than those in the HSSN-L group at 3 months after the surgery. These results indicated that the recovery of electrophysiological properties in HSSN-M and HSSN-H groups approached the autograft group prior to the HSSN-L group.

Histological analysis of myelinated axons, such as HE-staining and NF200/S100 immunofluorescence, further demonstrated the histological recovery in nerves bridged with HSSNs. HE staining images clearly confirmed that larger ISA/V of channels could strongly guide nerve regeneration. The NF200/S100 immunofluorescence images also demonstrated that the conduits with larger ISA/V have higher positive NF200 and S100 staining. These results were mainly attributed to the following reasons:[14,34] (1) larger ISA/V supplies adequate space for cell adhesion and promotes more nerve fibers to grow along with the rectilinear direction inside the channels; (2) larger ISA/V provides a conduit for diffusion of neurotrophic factors secreted by the damaged nerve stump; (3) larger ISA/V provides more support for the adherence of physiologically relevant Schwann cells and directional expansion of growing axons; and (4) HSSNs with a greater ISA/V possess a large network of interconnected pores that is conducive to transfer nutrients among the channels inside the HSSNs. Therefore, HSSN-M and HSSN-H can better support regeneration across the gaps by stabilizing the fibrin matrix and better guide regenerating axons.[35]

DOI: 10.1021/acsomega.7b01003
ACS Omega 2017, 2, 7471−7481

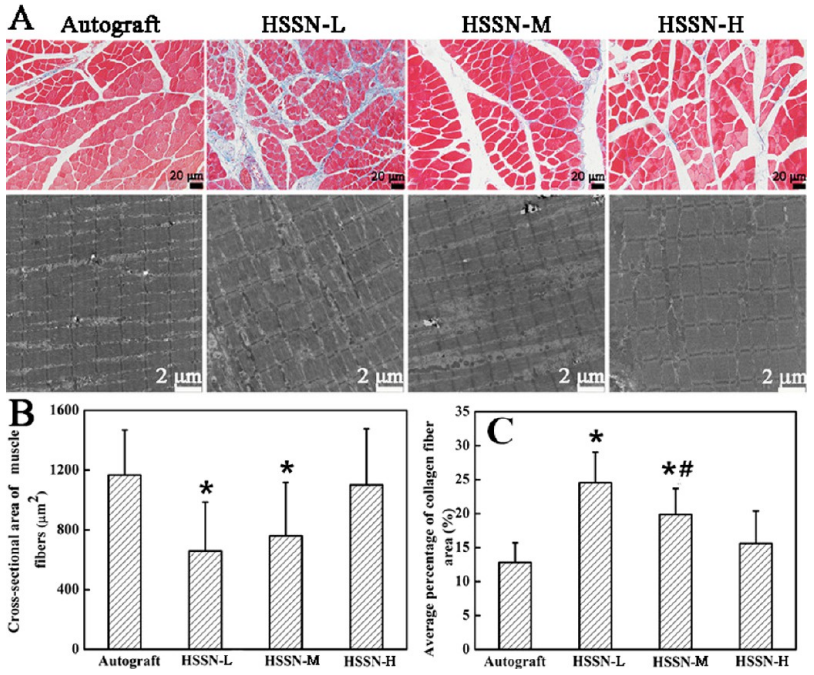

Figure 7. Masson trichrome staining of the cross-sections and TEM images of the longitudinal sections (A) of gastrocnemius muscle in each group at 3 months after the surgery. Cross-sectional area of muscle fibers (B) and average percentage of collagen fiber area (C) calculated from microscope images. White arrows present the wall among channels. * $P < 0.05$ (compared with autograft group); # $P < 0.05$ (compared with HSSN-L group). $n = 10$.

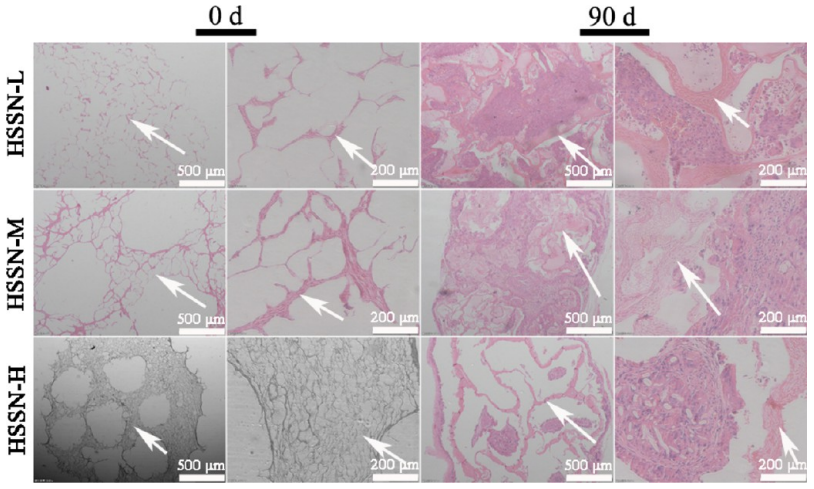

Figure 8. The HE images of biodegradability of HSSNs before and after implantation. White arrows present the wall among channels. 0 d: 0 day, 90 d: 90 days. $n = 10$.

Myelin sheath could not only support axons and adjacent tissues and avoid interference among axons but also guide axonal regeneration. Smaller diameter of the channel impeded connective tissue from occupying the internal space of channels. As a result, HSSNs with a larger ISA/V provided a greater and well internal environment for the regeneration, migration, and myelination of axons. As shown in toluidine blue staining and TEM analysis, the regenerative nerve tissues bridged with HSSN-H and HSSN-M showed larger axon diameter, lower *G*-ratio, and greater myelination thickness. Furthermore, the regenerative nerve tissues bridged with HSSN-H also showed higher density of regenerated myelinated nerve fibers and more number of myelin sheath layers. Meanwhile, more immature nerve fibers were observed in the HSSN-L group with smaller axon diameter and myelination thickness and less myelin sheath layers. The results of the CMAP test and histological evaluation revealed better microguide function of HSSN-M and HSSN-H with larger ISA/Vs.

As one of the most important nerves of animals, the sciatic nerve dominates all muscles of legs and feet. The natural nerve can bring normal sensory and motor functions, whereas the defected nerve leads to atrophy of the muscle fibers and hyperplasia in the connective tissues. As a result of motor nerve injury, denervation of a target muscle occurs, followed by alterations in a series of molecular events. This induces a shift in the protein metabolism from protein synthesis toward protein degradation and the decreased size of muscle fibers.[15] When reinnervation is achieved, the targeted muscle atrophy is stopped accompanied by a gradual functional recovery.[18,36,37] In this study, HSSN-M and HSSN-H better mimic the channel-

DOI: 10.1021/acsomega.7b01003
ACS Omega 2017, 2, 7471−7481

like complex architecture of native nerve tissues, exhibiting stronger microguide function and better nerve repair function owing to greater ISA/Vs than those of HSSN-L, hence better support the recovery of gastrocnemius muscle, such as the increased cross-sectional areas of muscle fibers, the decreased percentage of collagen fiber areas, and parallel muscle fibers of motor endplates.

Degradation capacity of biomaterials is an essential information required for tissue engineering NGC products.[38] In this case, we controlled the biodegradability of HSSNs by adjusting the epoxy chloropropane (ECH) content to match the rate of nerve regeneration as much as possible. As to the growth of the regenerative nerve, the higher degree of degradation resulted in thinner walls and produced larger lumen space for further growth. As a result, the larger lumen space provided a more advantageous microenvironment during the process of regeneration and promoted functional and histological recovery in the rat sciatic nerve defect. The mechanism may be attributed to its higher biomimetic effect. The biomimetic effect reduced the migration distance of the regenerating nerve and shortened the migration time of the regenerating nerve between proximal and distal stumps without decreasing the quantitative results of regeneration.

To date, the most effective way to repair large nerve defects still is autologous nerve grafting, which is regarded as the gold standard for peripheral nerve repair. Native nerve tissue consists of vast myelinated nerve fibers, which plays an important role in the peripheral nerve system. The nerve fibers could not only transmit electrical signals to adjust the metabolism of the nerve system but also release nutrition to promote the axonal growth and muscle operation. First, it is difficult to mimic the unique microstructure (channel-like architecture) of native nerve tissues. Second, unlike native nerve tissues, HSSNs lacked various matrix proteins, such as collagen and elastin. Third, the lack of integrated delivery systems for growth factors or facilitating cells (Schwann cells or stem cells) limited the nerve repair function.[18,27,39] Although HSSN-M and HSSN-H groups showed favorable repair function, the autograft group in our study still gave the best quantitative results of regeneration. Hence, we will further optimize the conditions with the addition of growth factors and seed cells in the future.

CONCLUSIONS

Three kinds of degradable NGCs with low, medium, and high ISA/Vs were fabricated from HEC/SPI-based sponges. The effect of the ISA/V on nerve regeneration was investigated. The overall results suggested that higher ISA/V was favorable to peripheral nerve regeneration. Thus, HSSN-M and HSSN-H with higher ISA/Vs may be potential alternatives in the repair of peripheral nerve defects. The conclusion provided a probable guiding principle for the structural design of MCNGCs in future.

EXPERIMENTAL SECTION

Materials. HEC was obtained from Shandong Head Co., Ltd. (Zibo, China). Commercial SPI was purchased from DuPont Zhengzhou Protein Technology Co. Ltd. (Zhengzhou, China). SPI was vacuum-dried for 24 h at 60 °C before use. Sodium hydroxide, ECH, and acetic acid were of analytical grade (Shanghai Chemical Reagent Co. Ltd, Shanghai, China).

Preparation of HEC/SPI Solution. HEC/SPI solution was prepared according to our previous method.[25] Briefly, a 2% HEC aqueous solution was prepared by dissolving HEC in deionized water. A 10% SPI aqueous solution was obtained by dispersing 10 g of SPI powders into 60 g of water, and then 30 g of NaOH aqueous solution (5%) were added to dissolve SPI. Then, HEC and SPI solutions were mixed mechanically to get HEC/SPI blend solution. Then, ECH (20% of the weight based on the total weight of the original SPI and HEC powders) was added dropwise in the blend solutions at room temperature under stirring for 30 min, which were further degassed at 10 °C by centrifugation for 10 min at 6000 rpm.

Fabrication of HEC/SPI Sponge-Based MCNGCs. A handmade mold was used to fabricate the HEC/SPI sponge-based MCNGCs.[40] First, 1, 3, and 7 stainless steel wires with diameters of 1.5, 0.8, and 0.5 mm, respectively, were evenly inserted into the handmade mold, and then the HEC/SPI solution was injected into the mold. The mold-containing HEC/SPI solution was frozen at −20 °C for 24 h and then was put into a precooled freeze dryer (Labconco Corp., Kansas City, MI, USA) to be freeze-dried for 24 h.[41] These freeze-dried sponges were removed from the molds and soaked into 5% acetic acid solution to neutralize NaOH and then rinsed with distilled water for 4 h. The sponges were freeze-dried again to obtain a series of HEC/SPI sponge-based NGCs with 12 mm length and coded as HSSN-L, HSSN-M, and HSSN-H, where L, M, and H mean low, medium, and high, respectively, corresponding to the surface area-to-volume ratio of channels in the conduits. For example, HSSN-L means the HEC/SPI sponge-based NGC with a low ISA/V in the channel. Figure 9 shows different views of HSSN-M and the schematic demonstration of ISA/V. Table 1 shows the conduits samples with various numbers, diameters, cross-sectional areas, volumes,

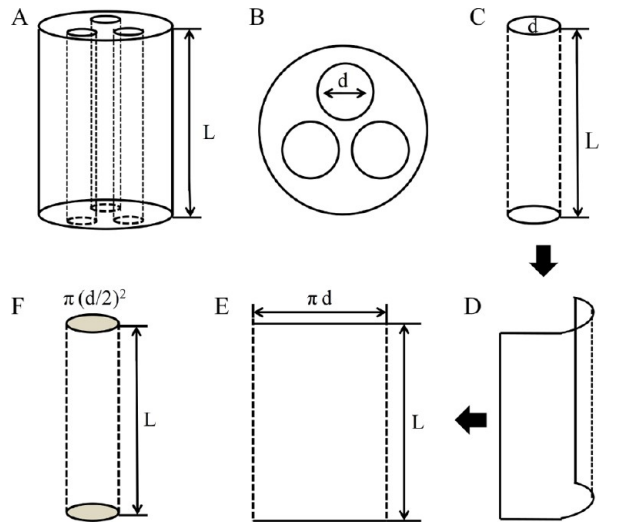

Figure 9. The schematic diagrams of side view (A) and cross-sectional view (B) of the HSSN-M. The schematic demonstration of the inner surface area (C-E) and the volume (F) of the single channel inside HSSN-M. To measure the inner surface area and the volume of the channels inside MCNGCs, a single channel was as an example to calculate the inner surface area and the volume. The diameter and length of a single channel inside MCNGCs were marked and noted by mouse clicks. Using a 2D image of unfolded inner surface of the channel to calculate the area according to the equation: Area = $\pi d \times L$. Afterwards, using a 3D image of the channel to calculate the volume according to the equation: Volume = $\pi(d/2)^2 \times L$.

DOI: 10.1021/acsomega.7b01003
ACS Omega 2017, 2, 7471−7481

inner surface areas, and surface area to volume ratios of channels in HSSNs.

Morphological Observation of HSSNs. To prepare samples for the observation of SEM, dried HSSN-L, HSSN-M, and HSSN-H were mounted on metal tabs using a carbon adhesive tape and then coated with gold. The whole appearance and cross sections were observed by SEM (VEGA 3 LMU, TESCAN, Czech Republic) at an accelerating voltage of 20 kV. Then, the pore size was measured according to SEM images. Briefly, 10 SEM images in each group were selected for pore size measurement. Three regions were randomly captured from every SEM image at 100× magnification and then analyzed with Image-Pro Plus software to measure the pore sizes of nerve conduits. First, we measured and recorded the maximum and minimum distances between any two sites along with the margin of a pore. Then, the average distance was calculated through averaging the maximum and minimum distances. The pore size was presented as the average distance.

Animal Experiments and Surgical Procedures for the Repair of Nerve Defects. The experiment was performed in compliance with the relevant laws and institutional guidelines such as Ministry of Science and Technology of the People's Republic of China "Guiding Opinions on the Treatment of Animals (09/30/2006)". All procedures concerning animals were approved by and conformed to the guidelines of the Animal Care & Welfare Committee of Wuhan University School of Medicine. Forty female adult Sprague Dawley rats, weighing approximately 200−220 g, were randomly divided into four groups (HSSN-L, HSSN-M, HSSN-H, and autograft groups) with 10 animals in each group. The surgery protocol was as follows: rats were anesthetized using 7% chloral hydrate solution (350 mg/kg body weight) by an intraperitoneal injection. The right sciatic nerve was exposed through an upper lateral thigh incision. A sciatic nerve segment was removed to create a 10 mm gap. The proximal and distal nerve ends were then inserted 1 mm into the 12 mm long conduits and were secured with 8-0 monofilament nylon sutures. For multichannel nerve conduits, before surgery, the spongelike channel walls within the multichannel nerve conduits at both ends of the multichannel conduits were removed using normal surgical tweezers. This could provide enough spaces for the accommodation of distal stump and proximal stump. After that, the proximal stump and distal stump of the transected peripheral nerve were placed at both ends of the conduit. The nerve stumps and conduit were then sutured together using 8-0 monofilament nylon sutures. For the autograft, the removed nerve segment was reversed 180° and reattached using 4-0 nylon sutures. The animals were returned to the cages where they had free access to food and water during a recovery period of 3 months.[42]

Electrophysiological Assessments. Three months after the surgery, the sciatic nerve on the operated side was re-exposed. Electrical stimulation was applied to the proximal nerve trunk, and the CMAP for the gastrocnemius belly on the operated side was recorded. Normal CMAPs were measured on the unoperated side.[18,32]

Histological Assessment of Regenerated Nerves. *HE Staining Analysis.* After conventional feeding for 3 months, the animals were deeply anesthetized after electrophysiological assessment. The regenerated nerve specimens were harvested, washed with phosphate-buffered saline (PBS), and fixed with 4% paraformaldehyde. Then, the tissues were dehydrated and embedded in paraffin. Longitudinal 5 μm sections were stained with hematoxylin/eosin (HE). The sections were observed using a light microscope (BX51, OLYMPUS, Japan).

Double NF200/S100 Immunofluorescence Analysis. For double immunofluorescence analysis of NF200 and S100, HSSNs and the regenerated nerves were dissected, fixed with 4% (w/v) paraformaldehyde at 4 °C for 6 h and then immersed for 3 days in 30 w/v % sucrose at 4 °C. Then, they were embedded with an optimal cutting temperature compound (Sakura, Tokyo, Japan) and frozen at −20 °C. Longitudinal sections with 10 μm thickness were prepared with a freezing microtome (CM1950, Leica, Germany). The sections were incubated with 1% normal goat serum in PBS (1 h, room temperature) and then with a mixture of primary antibodies, antiNF200 (1:500; ab24574; Abcam Inc., UK) and antiS100 (1:500; S2644, Sigma-Aldrich, USA). Afterward, the sections were rinsed in PBS and then incubated with a mixture of secondary antibodies, Alexa Fluor 594-conjugated goat antimouse IgG and Alexa Fluor 488-conjugated goat antirabbit IgG (1:500, Invitrogen, Carlsbad, CA, USA). Cell nuclei were stained with 4′,6-diamidino-2-phenylindole. Finally, the stained sections were rinsed and then viewed under a fluorescent microscope (BX51, OLYMPUS, Japan). Three images were captured randomly with an OLYMPUS DP71 digital camera at 200× magnification. These images were analyzed with Image-Pro Plus software to measure the positive NF200 and S100 staining area of the regenerated nerves. The original fluorescence image was inverted as a contrast, and then by discarding all color information, it was transformed into a gray-scale image. Afterward, the image was manually segmented according to the defined intensity range. The regions in the defined intensity range were selected. The selected regions were positive NF200 staining or positive S100 staining regions. Then, the total area of the selected regions and the total area of the image were measured with Image-Pro Plus software. Finally, the percentages of positive NF200 staining and positive S100 staining were calculated through dividing the positive area by the total area of the image.

Toluidine Blue Staining and TEM. After electrophysiological examination, the regenerated nerves or autografts were quickly harvested and fixed in cold buffered 2.5% glutaraldehyde solution for 6 h. Then, the regenerated nerves were washed with PBS, and sections were taken from the middle regions of the regenerated sciatic nerve. The samples were postfixed with 1% osmium tetraoxide solution, dehydrated, and embedded in an Epon 812 epoxy resin. Transverse semithin sections with a thickness of 1 μm were stained with toluidine blue and then observed under a light microscope (BX71, OLYMPUS, Japan). To quantify the density of myelinated nerve fibers, three images were randomly captured at 400× magnification for each nerve specimen and all these images were counted at 100× magnification to obtain the numbers of myelinated nerve fibers. Then, the number of myelinated nerve fibers per unit area was calculated for each image. The numbers of myelinated nerve fibers per unit area for three images were averaged to get the mean number of myelinated nerve fibers per unit area for each regenerated nerve. Then, the total number of myelinated nerve fibers for each regenerated nerve was calculated through multiplying the mean number of myelinated nerve fibers per unit area by the total area of myelinated nerve fibers. Transverse ultrathin 50 nm sections were stained with lead citrate and uranyl acetate and then examined under a transmission electron microscope (HT7700, Hitachi, Japan). Similarly, Image-Pro Plus software was used to measure axon

DOI: 10.1021/acsomega.7b01003
ACS Omega 2017, 2, 7471−7481

diameter, myelinated nerve fiber diameter, myelin sheath thickness, and the number of myelin sheath layer from the TEM images. For each specimen, four images were randomly captured at 700× magnification and 60 axons of each were randomly analyzed. The *G*-ratio was calculated according to the following formula.[43]

$$G\text{-ratio} = D_i/D_o \quad (1)$$

where D_o means the diameter of the corresponding fiber (outer) and D_i means the axon diameter (inner).

Histological Assessment of Gastrocnemius Muscles. Three months after the surgery, the gastrocnemius muscles of operated hind limbs were harvested and cut into halves. Half of the samples were fixed in 4% (w/v) paraformaldehyde in 0.1 mol/L phosphate buffer at 4 °C for 24 h and embedded in paraffin. Transverse 5 μm sections were prepared and subjected to Masson's trichrome staining and then observed under a light microscope (BX71, OLYMPUS, Japan). The other half of the samples were fixed in a buffered 2.5% glutaraldehyde solution, postfixed with 1% osmium tetraoxide solution, dehydrated, and embedded in an Epon 812 epoxy resin. Longitudinal ultrathin 50 nm sections were stained with lead citrate and uranyl acetate and examined under a transmission electron microscope (HT7700, Hitachi, Japan). To quantify the cross-sectional area of the muscle fibers and the percentage of the collagen fiber, three images were randomly captured at 200× magnification from each Masson's trichrome staining section and analyzed with Image-Pro Plus software. The cross-sectional area of the muscle fibers, the muscle fiber area (a), and the collagen fiber area (b) were measured from each image. The percentage of the collagen fiber (c) was calculated according to following formula.[15]

$$c\ (\%) = [b/(a+b)] \times 100 \quad (2)$$

Degradation of HSSNs. Three months after the surgery, HSSN-L, HSSN-M, and HSSN-H containing regenerated nerves were harvested, washed with PBS, and fixed with 4% paraformaldehyde for 24 h. Then, the samples were dehydrated using graded ethanol and embedded in paraffin. Transverse 5 μm sections were stained with HE. The sections were observed and photographed using a light microscope (BX71, OLYMPUS, Japan).

Statistical Analysis. All of the quantitative data were expressed as means ± standard deviation. Statistical comparisons were performed using one-way analysis of variance with Origin 8.0 software (OriginLab Co., Hampton, USA). *P* values of less than 0.05 were considered statistically significant.

AUTHOR INFORMATION

Corresponding Authors

*E-mail: liyinping@whu.edu.cn (Y.L.).
*E-mail: yunchen@whu.edu.cn (Y.C.).

ORCID

Yun Chen: 0000-0002-5984-7455

Author Contributions

Y.Z. and Q.Z. contributed equally to this work.

Notes

The authors declare no competing financial interest.

ACKNOWLEDGMENTS

This work was supported by the National Natural Science Foundation of China (grant nos. NSFC 81471789, NSFC 81171480, and 81270411). The authors acknowledge the help provided for electrophysiological assessment by the Experimental Teaching Center of Basic Medical Science, Wuhan University.

REFERENCES

(1) Cao, J.; Sun, C.; Zhao, H.; Xiao, Z.; Chen, B.; Gao, J.; Zheng, T.; Wu, W.; Wu, S.; Wang, J.; Dai, J. The use of laminin modified linear ordered collagen scaffolds loaded with laminin-binding ciliary neurotrophic factor for sciatic nerve regeneration in rats. *Biomaterials* **2011**, *32*, 3939−3948.

(2) Liao, C.; Huang, J.; Sun, S.; Xiao, B.; Zhou, N.; Yin, D.; Wan, Y. Multi-channel chitosan−polycaprolactone conduits embedded with microspheres for controlled release of nerve growth factor. *React. Funct. Polym.* **2013**, *73*, 149−159.

(3) Pabari, A.; Yang, S. Y.; Seifalian, A. M.; Mosahebi, A. Modern surgical management of peripheral nerve gap. *J. Plast. Reconstr. Aesthetic Surg.* **2010**, *63*, 1941−1948.

(4) Bellamkonda, R. V. Peripheral nerve regeneration: An opinion on channels, scaffolds and anisotropy. *Biomaterials* **2006**, *27*, 3515−3518.

(5) Cao, J.; Xiao, Z.; Jin, W.; Chen, B.; Meng, D.; Ding, W.; Han, S.; Hou, X.; Zhu, T.; Yuan, B.; Wang, J.; Liang, W.; Dai, J. Induction of rat facial nerve regeneration by functional collagen scaffolds. *Biomaterials* **2013**, *34*, 1302−1310.

(6) Dellon, A. L.; Mackinnon, S. E. An alternative to the classical nerve graft for the management of the short nerve gap. *Plast. Reconstr. Surg.* **1988**, *82*, 849−856.

(7) Tuinstra, H. M.; Aviles, M. O.; Shin, S.; Holland, S. J.; Zelivyanskaya, M. L.; Fast, A. G.; Ko, S. Y.; Margul, D. J.; Bartels, A. K.; Boehler, R. M.; Cummings, B. J.; Anderson, A. J.; Shea, L. D. Multifunctional, multichannel bridges that deliver neurotrophin encoding lentivirus for regeneration following spinal cord injury. *Biomaterials* **2012**, *33*, 1618−1626.

(8) Battiston, B.; Tos, P.; Conforti, L. G.; Geuna, S. Alternative techniques for peripheral nerve repair: conduits and end-to-side neurorrhaphy. *How To Improve the Results of Peripheral Nerve Surgery*; Acta Neurochirurgica Supplementum; Springer, 2007; Vol. *100*, pp 43−50.

(9) Gu, X.; Ding, F.; Yang, Y.; Liu, J. Construction of tissue engineered nerve grafts and their application in peripheral nerve regeneration. *Prog. Neurobiol.* **2011**, *93*, 204−230.

(10) Yao, L.; de Ruiter, G. C. W.; Wang, H.; Knight, A. M.; Spinner, R. J.; Yaszemski, M. J.; Windebank, A. J.; Pandit, A. Controlling dispersion of axonal regeneration using a multichannel collagen nerve conduit. *Biomaterials* **2010**, *31*, 5789−5797.

(11) Alluin, O.; Wittmann, C.; Marqueste, T.; Chabas, J.-F.; Garcia, S.; Lavaut, M. N.; Guinard, D.; Feron, F.; Decherchi, P. Functional recovery after peripheral nerve injury and implantation of a collagen guide. *Biomaterials* **2009**, *30*, 363−373.

(12) Wan, Y.; Huang, J.; Zhang, J.; Yin, D.; Zheng, Z.; Liao, C.; Sun, S. Investigation of mechanical properties and degradability of multi-channel chitosan−polycaprolactone/collagen conduits. *Polym. Degrad. Stab.* **2013**, *98*, 122−132.

(13) Moore, M. J.; Friedman, J. A.; Lewellyn, E. B.; Mantila, S. M.; Krych, A. J.; Ameenuddin, S.; Knight, A. M.; Lu, L.; Currier, B. L.; Spinner, R. J.; Marsh, R. W.; Windebank, A. J.; Yaszemski, M. J. Multiple-channel scaffolds to promote spinal cord axon regeneration. *Biomaterials* **2006**, *27*, 419−429.

(14) Bender, M. D.; Bennett, J. M.; Waddell, R. L.; Doctor, J. S.; Marra, K. G. Multi-channeled biodegradable polymer/CultiSpher composite nerve guides. *Biomaterials* **2004**, *25*, 1269−1278.

(15) Yang, Y.; De Laporte, L.; Rives, C. B.; Jang, J.-H.; Lin, W.-C.; Shull, K. R.; Shea, L. D. Neurotrophin releasing single and multiple lumen nerve conduits. *J. Controlled Release* **2005**, *104*, 433−446.

(16) Zhang, Q.; Zhao, Y.; Yan, S.; Yang, Y.; Zhao, H.; Li, M.; Lu, S.; Kaplan, D. L. Preparation of uniaxial multichannel silk fibroin scaffolds for guiding primary neurons. *Acta Biomater.* **2012**, *8*, 2628−2638.

DOI: 10.1021/acsomega.7b01003
ACS Omega 2017, 2, 7471−7481

(17) Tansey, K. E.; Seifert, J. L.; Botterman, B.; Delgado, M. R.; Romero, M. I. Peripheral Nerve Repair Through Multi-Luminal Biosynthetic Implants. *Ann. Biomed. Eng.* **2011**, *39*, 1815−1828.
(18) Yang, Y.; Ding, F.; Wu, J.; Hu, W.; Liu, J.; Gu, X. Development and evaluation of silk fibroin-based nerve grafts used for peripheral nerve regeneration. *Biomaterials* **2007**, *28*, 5526−5535.
(19) Zeng, C. G.; Xiong, Y.; Xie, G.; Dong, P.; Quan, D. Fabrication and evaluation of PLLA multichannel conduits with nanofibrous microstructure for the differentiation of NSCs in vitro. *Tissue Eng., Part A* **2014**, *20*, 1038−1048.
(20) Hadlock, T.; Sundback, C.; Hunter, D.; Cheney, M.; Vacanti, J. P. A Polymer Foam Conduit Seeded with Schwann Cells Promotes Guided Peripheral Nerve Regeneration. *Tissue Eng.* **2000**, *6*, 119−127.
(21) Park, S. J.; Lee, B.-K.; Na, M. H.; Kim, D. S. Melt-spun shaped fibers with enhanced surface effects: Fiber fabrication, characterization and application to woven scaffolds. *Acta Biomater.* **2013**, *9*, 7719−7726.
(22) Chew, S. A.; Arriaga, M. A.; Hinojosa, V. A. Effects of surface area to volume ratio of PLGA scaffolds with different architectures on scaffold degradation characteristics and drug release kinetics. *J. Biomed. Mater. Res., Part A* **2016**, *104*, 1202−1211.
(23) Scaglione, S.; Ceseracciu, L.; Aiello, M.; Coluccino, L.; Ferrazzo, F.; Giannoni, P.; Quarto, R. A Novel Scaffold Geometry for Chondral Applications: Theoretical Model and in Vivo Validation. *Biotechnol. Bioeng.* **2014**, *111*, 2107−2119.
(24) Li, X.; Zhao, T.; Sun, L.; Aifantis, K. E.; Fan, Y.; Feng, Q.; Cui, F.; Watari, F. The applications of conductive nanomaterials in the biomedical field. *J. Biomed. Mater. Res., Part A* **2015**, *104*, 322−339.
(25) Zhao, Y.; He, M.; Zhao, L.; Wang, S.; Li, Y.; Gan, L.; Li, M.; Xu, L.; Chang, P. R.; Anderson, D. P.; Chen, Y. Epichlorohydrin-Cross-linked Hydroxyethyl Cellulose/Soy Protein Isolate Composite Films as Biocompatible and Biodegradable Implants for Tissue Engineering. *ACS Appl. Mater. Interfaces* **2016**, *8*, 2781−2795.
(26) Gan, L.; Zhao, L.; Zhao, Y.; Li, K.; Tong, Z.; Yi, L.; Wang, X.; Li, Y. P.; Tian, W.; He, X.; Zhao, M.; Li, Y.; Chen, Y. Cellulose/soy protein composite-based nerve guidance conduits with designed microstructure for peripheral nerve regeneration. *J. Neural. Eng.* **2016**, *13*, 056019.
(27) Bozkurt, A.; Lassner, F.; O'Dey, D.; Deumens, R.; Böcker, A.; Schwendt, T.; Janzen, C.; Suschek, C. V.; Tolba, R.; Kobayashi, E.; Sellhaus, B.; Tholl, S.; Eummelen, L.; Schügner, F.; Damink, L. O.; Weis, J.; Brook, G. A.; Pallua, N. The role of microstructured and interconnected pore channels in a collagen-based nerve guide on axonal regeneration in peripheral nerves. *Biomaterials* **2012**, *33*, 1363−1375.
(28) Midha, R.; Munro, C. A.; Dalton, P. D.; Tator, C. H.; Shoichet, M. S. Growth factor enhancement of peripheral nerve regeneration through a novel synthetic hydrogel tube. *J. Neurosurg.* **2003**, *99*, 555−565.
(29) Laurencin, C. T.; Ambrosio, A. M. A.; Borden, M. D.; Cooper, J. A. Tissue engineering: orthopedic applications. *Annu. Rev. Biomed. Eng.* **1999**, *1*, 19−46.
(30) Woo, K. M.; Chen, V. J.; Ma, P. X. Nano-fibrous scaffolding architecture selectively enhances protein adsorption contributing to cell attachment. *J. Biomed. Mater. Res.* **2003**, *67*, 531−537.
(31) Jiao, H.; Yao, J.; Yang, Y.; Chen, X.; Lin, W.; Li, Y.; Gu, X.; Wang, X. Chitosan/polyglycolic acid nerve grafts for axon regeneration from prolonged axotomized neurons to chronically denervated segments. *Biomaterials* **2009**, *30*, 5004−5018.
(32) Ao, Q.; Fung, C.-K.; Tsui, A. Y.-P.; Cai, S.; Zuo, H.-C.; Chan, Y.-S.; Shum, D. K.-Y. The regeneration of transected sciatic nerves of adult rats using chitosan nerve conduits seeded with bone marrow stromal cell-derived Schwann cells. *Biomaterials* **2011**, *32*, 787−796.
(33) Matsumoto, K.; Ohnishi, K.; Kiyotani, T.; Sekine, T.; Ueda, H.; Nakamura, T.; Endo, K.; Shimizu, Y. Peripheral nerve regeneration across an 80-mm gap bridged by a polyglycolic acid (PGA)-collagen tube filled with laminin-coated collagen fibers: a histological and electrophysiological evaluation of regenerated nerves. *Brain Res.* **2000**, *868*, 315−328.
(34) Sundback, C.; Hadlock, T.; Cheney, M.; Vacanti, J. Manufacture of porous polymer nerve conduits by a novel low-pressure injection molding process. *Biomaterials* **2003**, *24*, 819−830.
(35) de Ruiter, G. C.; Spinner, R. J.; Malessy, M. J. A.; Moore, M. J.; Sorenson, E. J.; Currier, B. L.; Yaszemski, M. J.; Windebank, A. J. Accuracy of motor axon regeneration across autograft, single-lumen, and multichannel poly(lactic-co-glycolic acid) nerve tubes. *Neurosurgery* **2008**, *63*, 144−153.
(36) Bodine, S. C.; Latres, E.; Baumhueter, S.; Lai, V. K. M.; Nunez, L.; Clarke, B. A.; Poueymirou, W. T.; Panaro, F. J.; Na, E.; Dharmarajan, K.; Pan, Z. Q.; Valenzuela, D. M.; DeChiara, T. M.; Stitt, T. N.; Yancopoulos, G. D.; Glass, D. J. Identification of ubiquitin ligases required for skeletal muscle atrophy. *Science* **2001**, *294*, 1704−1708.
(37) Ijkema-Paassen, J.; Meek, M. F.; Gramsbergen, A. Transection of the sciatic nerve and reinnervation in adult rats: muscle and endplate morphology. *Equine Vet. J.* **2001**, *33*, 41−45.
(38) Hsu, S. H.; Chan, S. H.; Chiang, C. M.; Chen, C. C.; Jiang, C. F. Peripheral nerve regeneration using a microporous polylactic acid asymmetric conduit in a rabbit long-gap sciatic nerve transection model. *Biomaterials* **2011**, *32*, 3764−3775.
(39) Pfister, L. A.; Papaloïzos, M.; Merkle, H. P.; Gander, B. Nerve conduits and growth factor delivery in peripheral nerve repair. *J. Peripher. Nerv. Syst.* **2007**, *12*, 65−82.
(40) Chen, Y.; Zhao, L.; Gan, L.; Tong, Z.; Li, Y. P. Chinese Patent 201310674367.7, 2013.
(41) Luo, L. H.; Zhang, Y. F.; Wang, X. M.; Wan, Y.; Chang, P. R.; Anderson, D. P.; Chen, Y. Preparation, characterization, and in vitro and in vivo evaluation of cellulose/soy protein isolate composite sponges. *J. Biomater. Appl.* **2008**, *24*, 503−526.
(42) Zhu, S.; Ge, J.; Wang, Y.; Qi, F.; Ma, T.; Wang, M.; Yang, Y.; Liu, Z.; Huang, J.; Luo, Z. A synthetic oxygen carrier-olfactory ensheathing cell composition system for the promotion of sciatic nerve regeneration. *Biomaterials* **2014**, *35*, 1450−1461.
(43) Stang, F.; Fansa, H.; Wolf, G.; Reppin, M.; Keilhoff, G. Structural parameters of collagen nerve grafts influence peripheral nerve regeneration. *Biomaterials* **2005**, *26*, 3083−3091.

DOI: 10.1021/acsomega.7b01003
ACS Omega 2017, 2, 7471−7481